JACS
JOURNAL OF THE AMERICAN CHEMICAL SOCIETY
Article
pubs.acs.org/JACS

Altering the Static Dipole on Surfaces through Chemistry: Molecular Films of Zwitterionic Quinonoids

Lucie Routaboul,[†] Pierre Braunstein,*[,†] Jie Xiao,[‡] Zhengzheng Zhang,[‡] Peter A. Dowben,*[,‡] Guillaume Dalmas,[§] Victor Da Costa,[§] Olivier Félix,[∥] Gero Decher,[∥,⊥] Luis G. Rosa,[#] and Bernard Doudin*[,§]

[†]Laboratoire de Chimie de Coordination, Institut de Chimie (UMR 7177 CNRS), Université de Strasbourg, 4 rue Blaise Pascal, 67081 Strasbourg, France

[‡]Department of Physics and Astronomy, Nebraska Center for Materials and Nanoscience, University of Nebraska—Lincoln, Lincoln, Nebraska 68588, United States

[§]Institut de Physique et Chimie des Matériaux de Strasbourg (UMR 7504 CNRS), Université de Strasbourg, 23 rue du Loess, B.P. 43, 67034 Strasbourg, France

[∥]Institut Charles Sadron (UPR 22 CNRS), Université de Strasbourg, 23 rue du Loess, B.P. 84047, 67034 Strasbourg, France

[⊥]Faculté de Chimie, Université de Strasbourg, 1 rue Blaise Pascal, 67008 Strasbourg, France

[#]Department of Physics and Electronics, University of Puerto Rico—Humacao, 100 Road#908, CUH Station, Humacao, Puerto Rico 00791, United States

Supporting Information

ABSTRACT: The adsorption of molecular films made of small molecules with a large intrinsic electrical dipole has been explored. The data indicate that such dipolar molecules may be used for altering the interface dipole screening at the metal electrode interface in organic electronics. More specifically, we have investigated the surface electronic spectroscopic properties of zwitterionic molecules containing 12π electrons of the *p*-benzoquinonemonoimine type, $C_6H_2(\underline{\cdots}NHR)_2(\underline{\cdots}O)_2$ (R = H (**1**), *n*-C_4H_9 (**2**), C_3H_6–S–CH_3 (**3**), C_3H_6–O–CH_3 (**4**), CH_2–C_6H_5 (**5**)), adsorbed on Au. These molecules are stable zwitterions by virtue of the meta positions occupied by the nitrogen and oxygen substituents on the central ring, respectively. The structures of **2**–**4** have been determined by single crystal X-ray diffraction and indicate that in these molecules, two chemically connected but electronically not conjugated 6π electron subunits are present, which explains their strong dipolar character. We systematically observed that homogeneous molecular films with thickness as small as 1 nm were formed on Au, which fully cover the surface, even for a variety of R substituents. Preferential adsorption toward the patterned gold areas on SiO_2 substrates was found with **4**. Optimum self-assembling of **2** and **5** results in ordered close packed films, which exhibit n-type character, based on the position of the Fermi level close to the conduction band minimum, suggesting high conductivity properties. This new type of self-assembled molecular films offers interesting possibilities for engineering metal–organic interfaces, of critical importance for organic electronics.

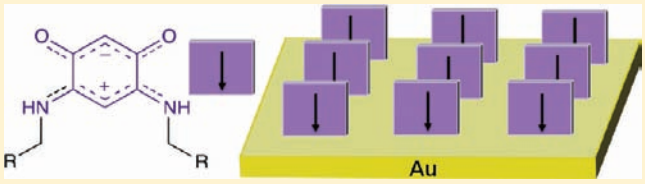

INTRODUCTION

Electronic properties at organic interfaces are of crucial importance for characterizing and understanding carrier injection and transport in organic electronics,[1,2] especially for the purpose of improving device properties.[3] The highest occupied molecular orbital (HOMO) and lowest unoccupied molecular orbital (LUMO) energy levels of free molecules are generally shifted when the molecules are brought into contact with a conducting substrate, and simple explanations based on vacuum levels alignment fail.[4] The fundamental reason is that the energy level alignment is dependent on the interfacial electronic structure and on interfacial dipole layer.[3,5,6] In most cases, when chemical interactions are not involved in the formation of an interfacial electronic structure, the Fermi level of the substrate should lie in the middle of the molecular adlayer HOMO–LUMO bandgap, consistent with the intrinsic dielectric properties of the bulk molecular material. With an interface dipole and charge transfer across the interface, molecular band offsets will occur, and this can then be exploited for improving molecular electronic device performance. The chemical bonding at the interface, the adsorbate molecular orientation,[7] the adsorbate dipole,[8,9] and their interplay[10,11] all play a role in establishing the interface dipole. This results in an interface potential barrier due to an offset between the conduction band minimum (LUMO) or the valence band maximum (HOMO) and the electrode Fermi level, leading to a charge injection barrier at the metal–molecules interface.[5,6] If the molecular species have a significant intrinsic dipole, one can expect an efficient screening of the

Received: January 6, 2012
Published: April 18, 2012

   dx.doi.org/10.1021/ja212104b | *J. Am. Chem. Soc.* 2012, 134, 8494–8506

ubiquitous metal−vacuum interface dipole, so that the molecular-type energy levels alignments remain invariant when decreasing the thickness of molecular adlayers.[5,12] The importance of controlling interface dipoles properties has been recently emphasized for organic spintronics applications, where spin-dependent charge transfer at the interface is the ingredient for optimizing device properties.[13] Furthermore, the intrinsic dipole of ferroelectric organic thin films on metallic electrodes has recently been reported as a way to improve the characteristics of devices.[14] Identifying families of dipolar molecules that are intrinsically good organic conductors, self-assemble well on metallic surfaces, and have enough flexibility in their design to allow many variations in pending or functional groups is therefore of key importance for a better understanding and mastering of the metal−organic interface.

In this paper, we report on our investigations of thin films made of small organic molecules with a large intrinsic dipole and significant flexibility in their design (Scheme 1). Although

Scheme 1. Resonance forms of the Zwitterionic Molecules Studied

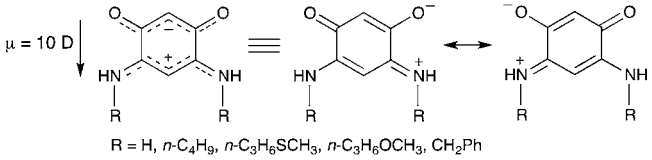

electrically neutral as a whole, these quinonomonoimines carry positive and negative charges on opposite parts of the molecule that are electronically isolated but chemically connected through carbon−carbon single bonds. The overall 12π electrons are thus partitioned in two 6π-electron subunits: the positive charge is delocalized between the nitrogen functions over four bonds involving 6π-electrons, while the negative charge is likewise spread between the oxygen atoms.[15,16] The resulting large electric dipole of typically 10 D over a short distance, formed across the planar six-membered ring structure of the *p*-benzoquinonemonoimine "core" (Scheme 1), should in principle maximize the electric field interacting with the surface.

Given the diversity and tunability of the chemical functions that can be incorporated in the pendant groups R attached to the quinonoid core without significant alterations of the strong intrinsic electric dipole (Scheme 2),[16−19] this is a very attractive

Scheme 2. Zwitterion Molecules with Different Pendant R Groups Studied

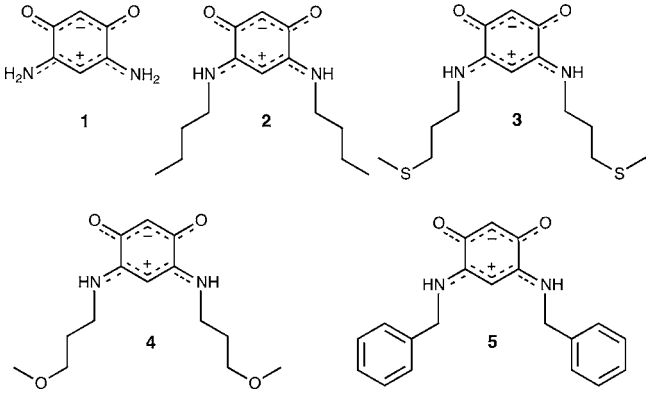

system for influencing the molecule−substrate interactions and possible self-assembled structures "by design".

Previous investigations on the electronic structure of *p*-benzoquinonemonoimine-type zwitterions focused on one particular compound: (6*Z*)-4-(butylamino)-6-(butyliminio)-3-oxocyclohexa-1,4-dien-1-olate, **2** (Scheme 2), that binds to Au substrates through the N functions (Scheme 3), with significant

Scheme 3. Model of the First Layer of Zwitterion 2 on a Au Surface

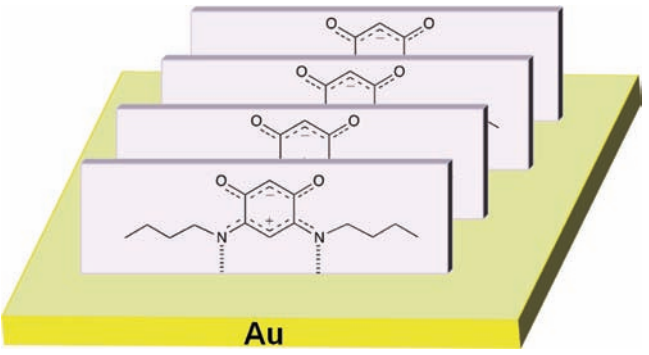

binding energy (0.5 eV) and forms uniform films of thicknesses down to the nanometer range.[20] The high symmetry corresponding to aligned molecular dipoles standing perpendicular to the substrate plane allows extensive use of surface spectroscopy selection rules and greater ease in the molecular vibrational mode assignments. Identification of fine spectroscopic structures (Franck−Condon substructures) was indeed successfully obtained.[20]

Engineering variations in the density and nature of the chemical attachment to a surface aim at gaining a better insight into the origin and control of the interface dipole.[5,6] This family of zwitterions thus provides a unique opportunity for systematic studies of self-assembly on surfaces and interface interactions, much like those studies undertaken for the metal(II) phthalocyanines,[8,21] or icosahedral *closo*-carboranes.[12] These *p*-benzoquinonemonoimines can also be used for surface functionalization purposes,[22a] as shown recently with the preferential adsorption of one isomer of diiodobenzene on the corresponding molecular films.[22b]

Several key general questions are to be addressed: does the creation of successful pinhole-free thin surface coverage require a strong chemisorption, are there pendant groups suitable for making crystalline surface packing possible, and how does the surface density of states compare to intrinsic molecular levels?

We will show here that the molecules selected (Scheme 2) are ideally suited to address these issues, owing to their unique dipolar character and their ability to self-organize through their electrostatic and H-bonding interactions. Ultrathin films of zwitterionic *p*-benzoquinonemonoimine compounds of good coverage are readily formed on Au. By varying the functional R group, chemisorption processes can be identified and electronic properties can be fine-tuned in relationship to the ability of the zwitterion to form close-packed crystalline structures. These ultrathin films systematically exhibit very efficient interface dipole screening, thus making the *p*-benzoquinonemonoimine-type zwitterionic compounds of interest owing to their interfacial electronic properties.

■ EXPERIMENTAL SECTION

Synthesis. *General.* Commercial 4,6-diaminoresorcinol dihydrochloride and functional amines were used directly

dx.doi.org/10.1021/ja212104b | *J. Am. Chem. Soc.* 2012, 134, 8494−8506

without further purification. Solvents were freshly distilled under argon prior to use. ^{1}H NMR spectra were recorded in $CDCl_3$ on a Bruker AC300 instrument, operating at 75 MHz for ^{13}C spectra and 300 MHz for ^{1}H spectra. Chemical shifts are in parts per million (ppm) relative to the singlet at δ = 7.26 for $CHCl_3$. The splittings are designated as s, singlet; d, doublet; t, triplet; m, multiplet; br, broad. Mass spectrometry experiments were performed on a Bruker Daltonics microTOF spectrometer (Bruker Daltonik GmbH, Bremen, Germany) equipped with an orthogonal electrospray (ESI) interface. Calibration was performed using Tunning mix (Agilent Technologies). Sample solutions were introduced into the spectrometer source with a syringe pump (Harvard type 55 1111; Harvard Apparatus, Inc., South Natick, MA) with a flow rate of 5 μL·min^{-1}. Elemental analyses were performed by the "Service de Microanalyse de l'Institut de Chimie" (Strasbourg, France).

Synthesis of (6*Z*)-4-(3(Methylthio)propylamino)-6-(3-(methylthio)propyliminio)-3-oxocyclohexa-1,4-dien-1-olate (3). *Method A.* 4,6-Diaminoresorcinol dihydrochloride (0.300 g, 1.41 mmol) was dissolved in a mixture of water and ethanol (5 mL/15 mL) and then 3-(methylthio)propylamine (1.1 mL, 9.81 mmol) was added to this solution. Immediately the color of the solution turned violet, and the solution was stirred for 2 h at room temperature in the presence of air. After concentration of the solution under reduced pressure, the residue was taken up in dichloromethane. The organic phase was dried over magnesium sulfate, and filtered through Celite. The solution was concentrated under reduced pressure and addition of pentane yielded the zwitterion **3** as a violet solid (0.410 g, 92%).

Method B. To a suspension of the parent zwitterion **1** (0.200 g, 1.45 mmol) in ethanol (10 mL) was added 3-(methylthio)propylamine (0.330 mL, 2.94 mmol). The mixture was refluxed for 2 h. After cooling to room temperature, the solution was filtered and evaporated to dryness under reduced pressure. The residue was taken up in dichloromethane and pentane was added to this solution to precipitate the product. After filtration, the zwitterion **3** was obtained as a violet solid (0.430 g, 94%). ^{1}H NMR (300 MHz, $CDCl_3$): δ = 2.03 (m, 4H, NCH_2CH_2), 2.12 (s, 6H, CH_3), 2.60 (t, $^3J_{HH}$ = 6.7 Hz, 4H, SCH_2), 3.56 (m, 4H, NCH_2), 5.38 (s, 1H, N···C···CH), 5.44 (s, 1H, O···C···CH), 8.44 (br s, 2H, NH). ^{13}C{^{1}H} NMR (75 MHz, $CDCl_3$): δ = 15.55 (s, CH_3), 27.28 (s, SCH_2), 31.23 (s, NCH_2CH_2), 41.74 (s, NCH_2), 80.91 (s, N···C···CH), 98.89 (s, O···C···CH), 157.04 (s, N···C), 172.29 (s, O···C). Mass spectrum: m/z: 315.1 $[M + 1]^+$. Anal. Calcd. for $C_{14}H_{22}N_2O_2S_2$: C, 53.47; H, 7.05; N, 8.91; S, 20.39. Found: C, 53.30; H, 6.85; N, 8.81; S, 20.64.

Synthesis of (6*Z*)-4-(3-Methoxypropylamino)-6-(3-methoxypropyliminio)-3-oxocyclohexa-1,4-dien-1-olate (4). *Method A.* 3-Methoxypropylamine (3.4 mL, 33.3 mmol) was added to a solution of 4,6-diaminoresorcinol dihydrochloride (1.00 g, 4.69 mmol) in water (10 mL). Within a few minutes, the color of the solution changed from brown to violet. After the reaction mixture was stirred for 2 h at room temperature in the presence of air, the product was extracted with dichloromethane. The organic layer was dried over magnesium sulfate, and filtered through Celite. The solution was concentrated under reduced pressure and addition of pentane precipitated the zwitterion **4** as a violet solid (1.05 g, 79%).

Method B. To a suspension of the parent zwitterion **1** (0.300 g, 2.17 mmol) in ethanol (15 mL) was added 3-methoxypropylamine (0.450 mL, 4.4 mmol). The solution was heated at 80 °C for 2 h. After cooling to room temperature, the solution was filtered and evaporated to dryness under reduced pressure. The residue was taken up in dichloromethane and pentane was added to this solution to precipitate the product. After filtration, the zwitterion **4** was obtained as a violet solid (0.541 g, 88%). ^{1}H NMR (300 MHz, $CDCl_3$): δ = 1.97 (m, 4H, NCH_2CH_2), 3.35 (s, 6H, CH_3), 3.46−3.52 (m, 8H, NCH_2 + OCH_2), 5.24 (s, 1H, N···C···CH), 5.43 (s, 1H, O···C···CH), 8.56 (br s, 2H, NH). ^{13}C{^{1}H} NMR (75 MHz, $CDCl_3$): δ = 28.3 (s, NCH_2CH_2), 41.09 (s, NCH_2), 58.91 (s, CH_3), 69.76 (s, OCH_2), 80.61 (s, N···C···CH), 98.94 (s, O···C···CH), 156.86 (s, N···C), 172.47 (s, O···C). Mass spectrum (Supporting Information): m/z 283.1 $[M + 1]^+$. Anal. Calcd. for $C_{14}H_{22}N_2O_4$: C, 59.56; H, 7.85; N, 9.92. Found: C, 59.26; H, 7.90; N, 10.12.

Crystal Structure Determinations. X-ray diffraction data were collected on a Kappa CCD diffractometer using graphite-monochromated Mo−Kα radiation (λ = 0.710 73 Å) (see Table S1 in the Supporting Information). Data were collected using ψ scans, the structures were solved by direct methods using the SHELX97 software,[23] and the refinement was by full-matrix least-squares on F^2. No absorption or self-absorption correction was used. All non-hydrogen atoms were refined anisotropically, with H atoms introduced as fixed contributors (d_{C-H} = 0.95 Å, $U11$ = 0.04). Crystallographic data (excluding structure factors) have been deposited in the Cambridge Crystallographic Data Centre as Supplementary Publication Nos. CCDC 814548, 814549 and 857868. Copies of the data can be obtained, free of charge, on application to the CCDC, 12 Union Road, Cambridge CB2 1EZ, U.K. (fax, (+44)-1223-336-033; e-mail, deposit@ccdc.cam.ac.uk).

Functionalization of Au Surfaces. Clean Au surfaces were obtained by e-beam evaporation, on Si/SiO_2 wafers, then washed successively with acetone and then ethanol in an ultrasound bath for 10 min each, and finally immersed in CH_2Cl_2. The zwitterionic molecules were deposited on the cleaned Au surfaces from a CH_2Cl_2 solution. Typical overnight exposure to a 0.8 mmol solution (0.2 g/L) was followed by ethanol washing to remove the excess molecules not bonded to the Au surface. The specifics of the cleaning process used for the preparation of the "thick" films were slightly modified to obtain the "thin" films.

"Thick" films: After the Au surface has been immersed at room temperature in the zwitterion solution for 16 h, it was taken out from the solution and immediately placed in a tube containing 3 mL of ethanol (in order to eliminate traces of the zwitterion solution from the Au surface). After 30 s, the Au surface was taken out and dried using a nitrogen gun, and the functionalized surface was kept under nitrogen atmosphere until measurements were performed.

"Thin" films: After the Au surface has been immersed at room temperature in the zwitterion solution for 16 h, it was taken out from the solution and immediately placed in a tube containing 3 mL of ethanol (in order to eliminate traces of the zwitterion solution from the Au surface). After 30 s, the Au surface was taken out, and placed again in a tube containing 3 mL of fresh ethanol for 1 min. This last washing was repeated twice, the surface was taken out and dried using a nitrogen gun, and the functionalized surface was kept under nitrogen atmosphere until measurements were performed. These simple sample preparation and cleaning methods led to highly reproducible results. Films of decreasing thickness were obtained by repeating the ethanol immersion step described above.

Monitoring of Molecular Film Growth. The assembly of molecular films on Au was investigated in real time by quartz crystal microbalance with dissipation monitoring (QCM-D). The QCM-D experiments were carried out in flow mode using a Q-Sense E4 instrument equipped with a flow module (QFM 401) (Q-Sense AB, Sweden). AT-cut quartz crystals with a fundamental frequency of 5 MHz, coated with Au or SiO_2, were purchased from Q-Sense AB (Sweden). The QCM-D technique may be briefly described as: upon adsorption of matter on the surface of a sensor crystal, changes in resonance frequency, Δf, and in dissipation, ΔD, are measured with a time resolution better than 1 s. Δf and ΔD are related to the mass of the adsorbed layer and to the viscoelastic properties of the adsorbed layer, respectively. Δf and ΔD values were measured at several harmonics (15, 25, 35, 45, 55, and 65 MHz) simultaneously. Changes in the normalized frequency ($\Delta F_{norm} = \Delta f_n/n$, where n is the harmonic number) and in dissipation of the seventh overtone (n = 7, i.e., 35 MHz) are presented. The adsorbed mass, m, was calculated according to the Sauerbrey equation,

$$m = -C \cdot \Delta F_{norm}, \quad \text{with} \quad C = 17.7 \text{ ng cm}^{-2} \text{ Hz}^{-1}$$

Prior to use, the crystals were cleaned by an UV-ozone treatment for 15 min (ozone removes organic carbon contamination). Experiments were carried out at 22 °C using a flow rate of 0.3 mL/min. After stabilization of the baseline, ethanol (EtOH) was replaced by 0.6 mL of a solution containing the corresponding zwitterion and adsorption on the surface was monitored. Finally, the resulting layer was rinsed several times with EtOH. Data (f and D) were collected continuously as a function of time.

Atomic Force Microscopy (AFM). AFM measurements were performed with a commercial D3100 setup from Veeco company. Images were acquired on a tapping mode (noncontact mode) using commercial Si tips (Nanosensors). Typical scan rate of the tip over the surface is 1 Hz.

Spectroscopic Surface Studies. Core level X-ray photoemission spectra (XPS) were taken with a SPECS X-ray source with a Mg anode ($h\nu$ = 1253.6 eV). Combined ultraviolet photoemission (UPS) and inverse photoemission (IPES) spectra of molecules **1**−**5** were taken on Au substrates in a single ultrahigh vacuum chamber. The IPES data were obtained using variable incident energy electrons while detecting the emitted photons at a fixed energy (9.7 eV) using a Geiger-Müller detector. This spectroscopy was limited by an instrument line width of ca. 400 meV. The angle-integrated UPS studies were carried out using a helium lamp at $h\nu$ = 21.2 eV (He I) and a Phi hemispherical electron analyzer with an angular acceptance of ±10° or more. For molecules **2** and **5**, additional photoemission measurements were taken, both angle-resolved and for different photon energies. These angle-resolved photoemission spectroscopy (PES) measurements employed plane-polarized synchrotron radiation dispersed by a 3 m toroidal grating monochromator at the Center for Advanced Microstructures and Devices (CAMD). The measurements were made in a UHV chamber employing a hemispherical electron analyzer with an angular acceptance of ±1°. The combined resolution of the electron energy analyzer and monochromator was in the range 70−120 meV. In both photoemission and inverse photoemission measurements, the binding energies are referenced with respect to the Fermi edge (E_F = 0 eV) of Au in intimate contact with the sample surface, in terms of $E - E_F$ (thus making occupied state energies negative). As noted throughout, valence band spectra do not show the valence band Au features after the deposition of the zwitterion thin films, but the core level Au signal has been observed and exploited, a common and widely used technique.[24] These Au 4d and 4f core level intensities were one of several measures used to estimate film thickness. They are not always accurate, on an absolute scale, because of uncertainties in the electron mean free path, but valuable for comparing films according to the relative film thickness.

The infrared (IR) microspectroscopy[25] measurements for the *p*-benzoquinonemonoimine zwitterions adsorbed on Au were carried out at the same synchrotron facility used for angle-resolved photoemission spectroscopy and high resolution photoemission, by means of the IR reflection mode of Thermo Nicolet continuum microscope.

Molecular Orbital Calculations. Calculations of the molecular orbitals, both occupied and unoccupied, of molecular films were performed for comparison purposes with the density of states deduced from the UPS-IPES experiments. The simple single molecule calculated density of states (as in a gas phase experiment), or molecular orbital theory (MOT), used semiempirical methods NDO-PM3 (neglect of differential diatomic overlap, parametric model number 3) based on Hartree−Fock formalism. Geometry optimization for each of the *p*-benzoquinonemonoimine zwitterion systems was performed by obtaining the lowest restricted Hartree−Fock energy states. The calculated density of states (DOS) were obtained by applying equal Gaussian envelopes of 1 eV full width half-maximum to each molecular orbital to account for the solid state broadening in photoemission and then summing. This model density of states calculations were rigidly shifted in energy, largely to account for the influence of work function on the orbital energies and no correction was made for molecular interactions and final state effects.

More sophisticated calculations included intermolecular effects so the result is effectively a band structure type calculation (BT) based on a lattice of zwitterion molecules. DFT first-principles calculations as implemented in the DMol^3 code were performed.[26] The PW91 generalized gradient approximation (GGA) was used for the exchange-correlation functional because of the better performance of GGA than the local density approximation (LDA) in many molecular systems. All the electrons were considered equally, and the double numerical plus polarization (DNP) basis set, which is comparable to the 6-31G** basis set, was used. The convergence tolerance for the self-consistent field is 2.72 × 10^{-6} eV, and the molecular structures were optimized until the maximum force was below 0.054 eV/Å.

RESULTS AND DISCUSSION

Synthesis and Characterization. The zwitterions **1**, **2**, and **5** (Scheme 2) were synthesized according to established procedures,[18] and molecules **3** and **4** were synthesized using two methods: (A) by a "one pot synthesis", in which amine addition to a suspension of diaminoresorcinol dihydrochloride in ethanol smoothly yielded the zwitterions; or (B) by a trans-amination reaction between a primary amine and the "parent zwitterion" **1** (Scheme 4).[18,19]

Scheme 4. Synthetic Methods Leading to Zwitterions 3 and 4

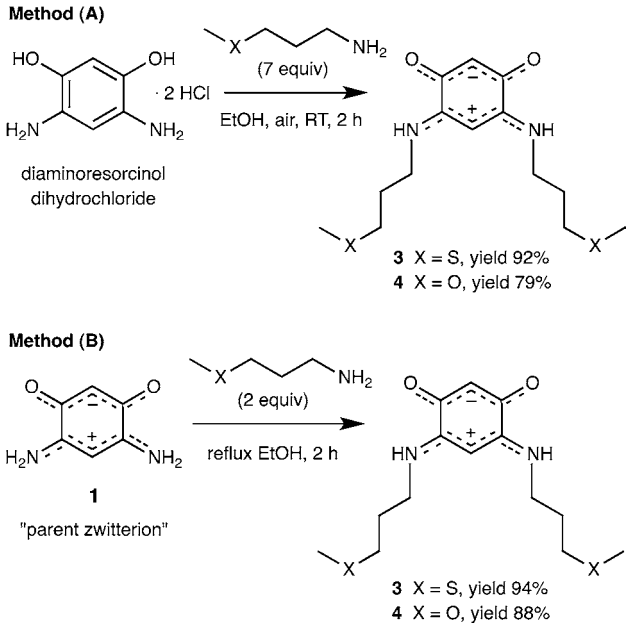

The yields of both reactions are good to excellent and the pure zwitterions were readily isolated. Method (A) allows the use of commercially available reagents and is easily scaled up. In method (B), the stable "parent zwitterion" **1**, which is also available in multigram quantities, can be quantitatively converted to the desired products within 2 h by using stoichiometric amounts of amine, which is advantageous in case the latter is expensive.

Single crystals of zwitterions **2**−**4** suitable for X-ray diffraction were obtained at room temperature by slow diffusion of pentane into their dichloromethane solution. Details on the refinement results are given in the Supporting Information (Table S1). The molecular structure of **3** is shown in Figure 1, those of **2** and **4** are very similar and shown in Figures S9 and S10, respectively, of the Supporting Information.

The experimentally determined bond lengths of the molecule C_6 core are summarized in Table 1. They are similar to those observed in the structures of related zwitterions.[16,18,19] Most

dx.doi.org/10.1021/ja212104b | J. Am. Chem. Soc. 2012, 134, 8494−8506

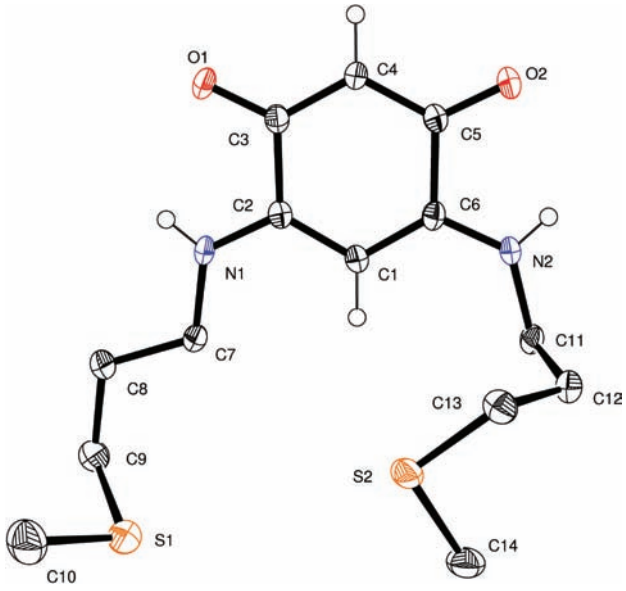

Figure 1. ORTEP of **3**. Thermal ellipsoids are drawn at the 40% probability level. H atoms on the thioether chain are not shown for clarity.

Table 1. Interatomic Distances (Å) Observed in Zwitterions 2–4

Zwitterion **2**		Zwitterion **3**		Zwitterion **4**	
C(3)–C(4)	1.395(3)	C(3)–C(4)	1.405(5)	C(3)–C(4)	1.393(2)
C(4)–C(5)	1.392(3)	C(4)–C(5)	1.393(5)	C(4)–C(5)	1.392(2)
C(3)–C(2)	1.518(3)	C(3)–C(2)	1.513(5)	C(3)–C(2)	1.522(2)
C(5)–C(6)	1.517(3)	C(5)–C(6)	1.531(5)	C(5)–C(6)	1.526(2)
C(1)–C(2)	1.384(3)	C(1)–C(2)	1.386(5)	C(1)–C(2)	1.388(2)
C(1)–C(6)	1.393(3)	C(1)–C(6)	1.392(5)	C(1)–C(6)	1.389(2)
C(3)–O(1)	1.253(3)	C(3)–O(1)	1.253(4)	C(3)–O(1)	1.249(2)
C(5)–O(2)	1.254(3)	C(5)–O(2)	1.256(4)	C(5)–O(2)	1.247(2)
C(2)–N(1)	1.317(3)	C(2)–N(1)	1.326(5)	C(2)–N(1)	1.319(2)
C(6)–N(2)	1.319(3)	C(6)–N(2)	1.313(5)	C(6)–N(2)	1.318(2)

significantly, the bond lengths C(3)–C(4)/C(4)–C(5) and C(3)–O(1)/C(5)–O(2), respectively, are almost equal. Likewise C(1)–C(6)/C(1)–C(2) as well as C(2)–N(1)/C(6)–N(2) are similar, respectively (Table 1). Their values are intermediate between those for single and double bonds. However, the C(2)–C(3) and C(5)–C(6) distances are much longer and are consistent with single bonds. On the basis of these metrical data, these zwitterions are well described as two fully delocalized 6π electrons systems (trimethyne oxonol part, O···C···CH···C···O, and the trimethyne cyanine part, N···C···CH···C···N) connected by two C–C single bonds.[16,18,19]

The strong molecular dipole moment and the presence of hydrogen bonds between adjacent zwitterions results in their head-to-tail arrangement (Figure 2) and the formation of a well-organized 1-D ribbon structure, with a repeat unit of ca. 14.9 Å. Furthermore, Figure 3 shows that parallel zwitterionic molecules **3** also pack in a direction transverse to the C_6 core, with a spacing of 3.24 Å. A similar value (3.38 Å) is found for molecule **4** (see Supporting Information Figure S11) while the packing of molecule **2** is more complicated, keeping however an average spacing of ca. 3.5 Å (see Supporting Information Figure S12). 2-D supramolecular networks therefore result from H-bonding and π-stacking interactions, forming "layers" of molecules (see Figure 3 illustrating the packing of these layers). These layers are separated by ca. 10 Å, slightly more in the case of **2** (12.6 Å) (Supporting Information Figure S12) and **3** (14.9 Å) (Figure 3), than in the case of **4** (9.3 Å) (Supporting Information Figure S11). If zwitterionic thin films preserve the ability to self-organize, we can expect that ordered molecular films can be formed on Au surfaces.

Since thiol or disulfide functionalities are among the most obvious choices for strengthening molecular anchoring on Au, according to the extensive literature on self-assembled monolayers,[27,28] we attempted to isolate pure zwitterions **6** and **7** (Scheme 5), but failed (details provided in Supporting Information).

We therefore investigated zwitterions with terminal thioether groups (molecule **3**), which are easier to synthesize and more stable toward oxidation than the thiol or disulfide analogs. Their successful attachment to Au, especially when weaker interactions are needed, as in the case of molecular rotors, has been reported by several groups.[29−32] XPS studies of thioether zwitterion **3** on Au revealed, however, significant decomposition caused by high fluences of low energy electrons and possibly other irradiation. The fact that we did not observe any evidence of decomposition of the butyl zwitterion **2** on Au (although much care was given to keeping the total fluences low) suggests that S–C bonds may be the weakest part of the molecule after adsorption.[33,35b] To confirm this assumption, we synthesized the zwitterion **4** which differs from **3** only by the replacement of sulfur with oxygen. Interestingly, zwitterion **4** is much more soluble in water than **3**.

Adsorption on Surfaces. The *p*-benzoquinonemonoimine zwitterions **2–4** were deposited on clean Au substrates from CH_2Cl_2 or EtOH solutions, and the zwitterions **1** and **5** from CH_2Cl_2 solutions only, owing to their poor solubility in EtOH. Quartz crystal microbalance with dissipation monitoring (QCM-D) experiments were performed to estimate the adsorbed mass of the layer and the kinetics of surface adsorption. We used a commercial system (QCM-E4, Q-Sense AB, Sweden) that allows for 4 parallel experiments, thus providing greater confidence in the reproducibility and facilitating comparisons between molecules. Figure 4 shows the frequency changes as a function of time upon formation of the molecular films of zwitterions **2** and **4**.

While several injections were necessary for zwitterion **4** to obtain a maximum number of molecules adsorbed on the surface, one injection was sufficient for zwitterion **2**. Successive EtOH washings can eliminate a significant fraction of the deposit, especially in the case of zwitterion **4**, where approximately half of the adsorbed molecules are removed from the surface by rinsing. However, after extensive washing, the residual QCM-D frequency shifts and the low dissipation values, in the same order of magnitude for both cases, indicate a remarkably stable thin molecular adsorption (Figure 4, inset). As an example, the thickness of molecule **2** on Au can be estimated using an approximate model of molecular packing on the surface, inspired by the findings described in the next sections. We propose that each molecule fills a cell of roughly 3.5 × 17 Å (dipole normal to the surface, π–π stacking with a spacing of 3.2 ± 0.2 Å and molecule length of 17 Å). The observed change of frequency (after overnight dipping and extensive cleaning) ranges from 4 to 8 Hz on four samples. Using the Sauerbrey equation, the frequency change corresponds to a coverage of 1–2 layers of molecules. We therefore deduce that a thin film adsorbs rather rapidly, with the typical

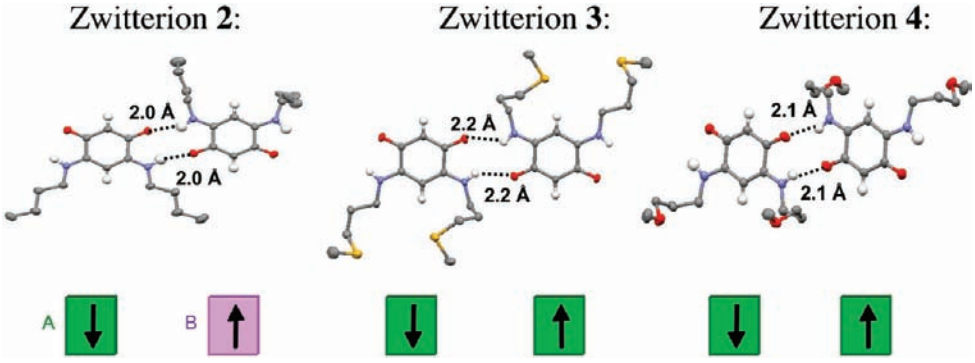

Figure 2. Head-to-tail arrangement of the zwitterion molecules **2**–**4** in the crystalline state, resulting from H-bonding and electrostatic interactions. The arrows indicate the dipoles directions. For compound **2**, there are two molecules A and B which only differ by the conformation of the butyl chains in the asymmetric unit, as illustrated by the color coding.

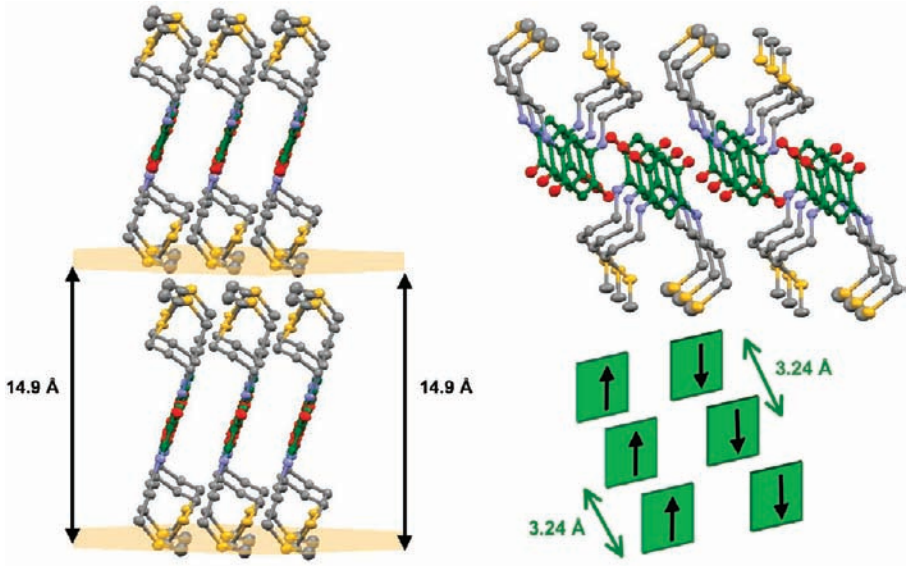

Figure 3. Packing of molecules **3**. (Left panel) The spacing of 14.9 Å between two 1D-ribbons is taken as the maximum separation between the mean planes containing the S atoms. (Right panel) View showing rows of parallel molecules separated by 3.24 Å.

Scheme 5. Thiol- or Disulfide-Functionalized Zwitterions

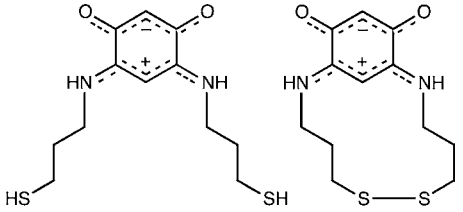

6 **7**

isothermal adsorption saturating within tens of minutes. Subsequent adsorption and increasing layer thickness are slower and may involve reorganization of the adsorbed film. Washing of the sample with a flow of EtOH removes a significant fraction of the deposit that occurred after the first 20 min of immersion. Data of Figure 4 indicate that the remaining fraction depends on the type of molecule studied, suggesting that longer immersion time improves film packing. The differences in adsorption between zwitterions **2** and **4** can be related to the better crystal packing observed for **2** (see next sections). For the thickness dependence data shown in the

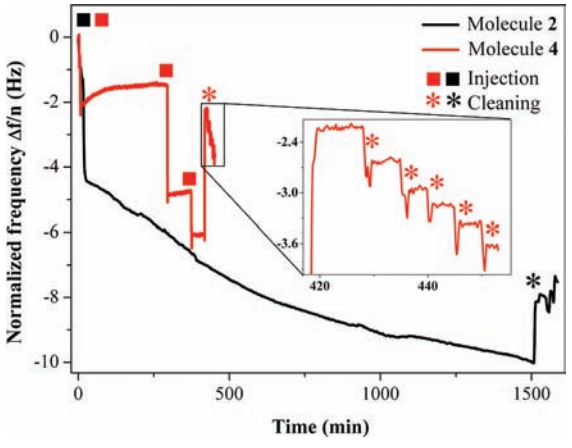

Figure 4. Evolution of the normalized frequency, measured at 35 MHz by QCM-D, as a function of time for the adsorption of zwitterions **2** (black) and **4** (red) on Au. Squares indicate zwitterion injections and asterisks correspond to EtOH rinsing steps. The inset is a magnification revealing the negligible change of the adsorbate mass after multiple rinsing steps (with the residual measurement drift related to repetitive changes in the sample environment).

dx.doi.org/10.1021/ja212104b | J. Am. Chem. Soc. 2012, 134, 8494–8506

subsequent sections, we therefore typically used overnight dipping of the substrate in the solution, and multiple gentle washing cycles to obtain films of decreasing thickness.

The QCM-D studies were also performed on substrates other than Au, confirming that the butyl zwitterion **2** can also be adsorbed on SiO_2. The observed changes of the QCM-D frequency were, however, smaller than those observed on Au, indicating the formation of less dense layers.

Atomic force microscopy (AFM) imaging was performed on atomically flat mica substrates (Figure 5). We found that mica

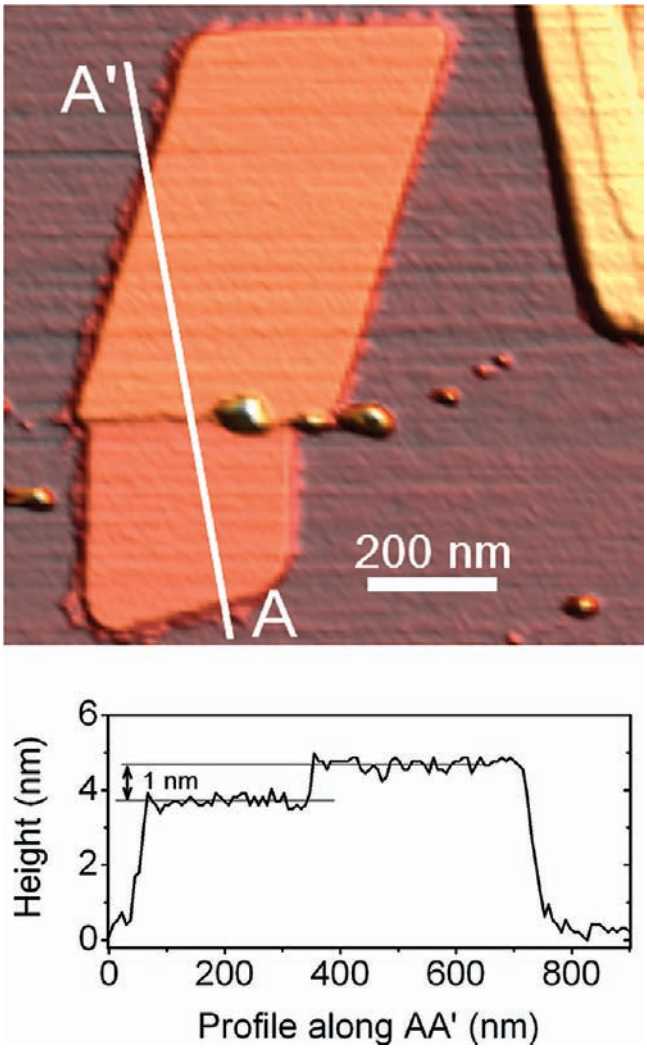

Figure 5. Atomic force microscopy mapping of zwitterion **2** adsorbed on mica. The topography scan reveals thin crystals, in the 3−7 nm thickness range. They exhibit 1 nm steps, which correspond to bimolecular layer thickness (see Supporting Information Figure S12). Note that the top right crystal shows identical step height.

was a convenient flat substrate where nonuniform covering of the molecules can occur. Partial coverage can be identified on a few selected areas only, with imaging revealing the growth of thin flat crystals made of a few molecular layers, with steps of the order of 10 Å, a value similar to the layer thickness of molecule **2** (Supporting Information Figure S12). This suggests that the 2-D arrangement of the zwitterions present in the crystalline state (Supporting Information Figure S12) may be retained in thin dense packings on surfaces.

Bonding to the Substrate. Partial insight into the molecule−substrate interactions was gained from the XPS data. We found that the molecules are stable on the time scale of the spectroscopy measurements, except in the case of molecule **3**, found to be the least surface stable among the compounds studied. This molecule rapidly dissociates under electron irradiation and the time evolution of the IPES provides indications of a negative ion resonance state at about 2 eV above the Fermi level (associated with an unoccupied molecular orbital state). Such negative ion resonance states in this energy region are typical for alkyl−sulfur bond dissociation (for vertical attachment into the σ^*(C−S) orbital, the energy is 3.2 eV).[33] We have good reasons to believe that zwitterion **3** adsorbs on Au as intact molecules (i.e., do *not* initially dissociate), but the electrons generated in electron spectroscopies can cause or enhance their dissociation, or molecular fragmentation may be substrate mediated, that is to say, fragmentation is enhanced at finite temperatures because of the conducting substrate. The dissociation outcome is difficult to identify: one possibility is the Au substrate-promoted rupture of the two C−S bonds. We therefore resorted to very low photon fluxes in X-ray photoemission throughout these investigations, at the expense of the signal-to-noise ratio, but the X-ray photoemission results are very reproducible. Unambiguous indications of bonding through the iminium/enamine groups have been previously provided in the case of butyl R groups (molecule **2**).[20] The N 1s core level shift of 0.5 ± 0.2 eV for **2**[20] is not observed when the thickness of the molecular films of **3** or **4** on Au was increased (see Supporting Information), suggesting that no chemisorption through the nitrogen atoms occurs for these molecules. The binding energies (Supporting Information Figure S13) are in line with the expected N 1s core levels for related organic compounds with amine and amide groups.[34]

A clear S $2p_{3/2}$ core level shift with increasing coverage is found for molecule **3** with the pendant thioether groups (Figure 6). The binding energy shift of 1.1 ± 0.1 eV (−162.3 ± 0.2 to −163.4 ± 0.2 eV for the S $2p_{3/2}$) is larger, but similar in character to the N 1s core level shift observed for zwitterion **2**. We interpret these core level shifts as indicative of binding of the molecule to Au largely through S, in the thin film limit. We cannot exclude here bonding through the iminium/enamine groups, but if such bonding occurs, it is very weak. Oxidation of a thiolate end group still attached to an alkane or organic fragment is unlikely, as it should relate to a binding energy of 166 eV,[35] not observed. The S $2p_{3/2}$ core level binding energies (−161.7 ± 0.2 eV) are in good agreement with the S core level binding energies of −161.8 eV observed for alkane thiol self-assembled monolayers on Au,[27] and of −162.1 eV for benzyl dithiobenzoate[31] or biphenylthiol self-assembled monolayers on Au.[32] The binding energy at −162.9 ± 0.2 eV for the S $2p_{3/2}$ level seen for higher coverages is characteristic of free thiols not bound to the metal (−163 eV).[27]

We thus found indications of surface bonding for molecules **2** and **3**, establishing that the chemisorption of quinonoid zwitterions on Au is not limited to molecules with an alkyl N-substituent, as in **2**. Direct XPS evidence of significant binding energies shifts of several hundreds of millielectronvolts (meV) for molecules **1**, **4**, and **5** is however lacking, and a whole host of reasons for this can be invoked which include a complex distribution of bonding with the substrate, weak interactions with the substrate, or a signal not easily abstracted from other N, O, or C core level spectroscopic components.

dx.doi.org/10.1021/ja212104b | J. Am. Chem. Soc. 2012, 134, 8494−8506

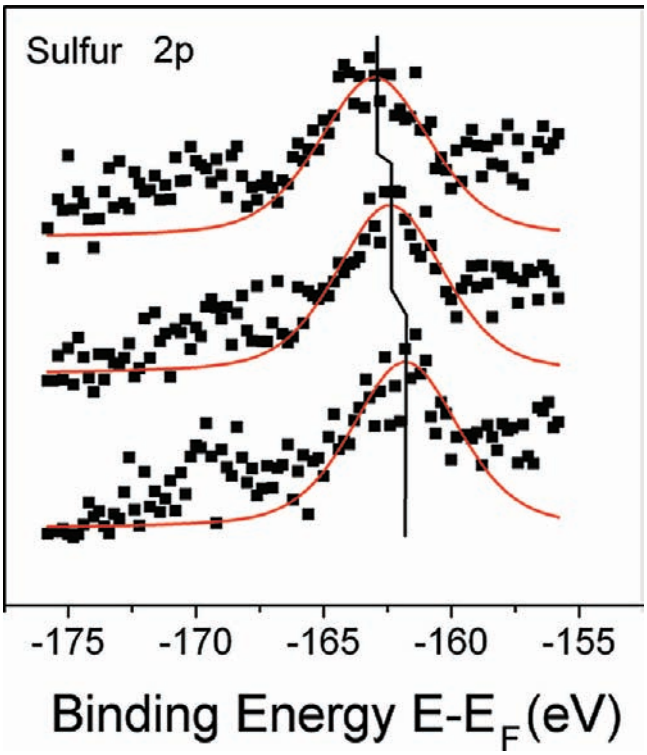

Figure 6. The S 2p core levels X-ray photoemission spectra with increasing coverages on Au of the thioether-functionalized *p*-benzoquinonemonoimine zwitterion (molecule **3**). The main peak shifts are indicated by vertical bars, set at the maxima of a Gaussian fit of the spectra. The sulfur 2p component at 169 eV binding energy is a photoemission shake up satellite common to many adsorbed zwitterions of this class (see text).

Electronic Properties. The surface electronic structure properties were investigated using a combination of UPS and IPES spectra, taken in a single ultrahigh vacuum chamber to characterize the placement of both occupied and unoccupied molecular orbitals of the adsorbates as a function of film coverage (thickness).

The changes in relative film thickness, as denoted in Figure 7, are related to successive washing cycles, and have been confirmed by valence band and core level photoemission. In particular, the decrease in film thickness with an increase in the number of washing cycles corresponds to the observed increase of the Au 4d core level photoemission intensity, as expected. Details of the data are shown in Figure S14 of the Supporting Information). Note that the absolute value of the thickness cannot be unambiguously determined, while the Au 4f photoemission monitoring provides confidence in the sequence of thickness values. We found a very good reproducibility of the data, and a similar spectra sequence was found when varying the washing process (flow of solvent, use of alternative solvent for washing), providing confidence in the robustness of our results. The Au surface core level signals of the buried interface indicate that we reach, after cleanings, organic films less than 3 nm thick. The occurrence of metal-induced gap states revealed by small features within the HOMO−LUMO bandgap[20] should become extinct for a thickness greater than 2 nm, because of the very short mean free paths of the low energy electrons detected in photoemission experiments. No indication of bare Au valence or conduction band spectroscopic features was found for all thicknesses and all species of Figure 8, where comparison spectra are shown for molecules **1**−**5**. We therefore estimate that typically more than 98% of the Au surface is covered. This provides strong evidence that the molecular films cover the substrate remarkably well.

When combining the evidence of good coverage (pinhole free molecular films) with the QCM-D information which provides an estimate of the weight increase related to the thinnest films, we can conclude that molecular films, as thin as 1 nm, can possibly form (at least for molecules **2** and **4**), reaching the single to double layer coverage.

The experimental spectra of Figures 7 and 8 were compared with a simple single molecule calculated density of states (MOT). These calculations were rigidly shifted in energy, largely to account for the influence of work function on the orbital energies and no correction was made for molecular interactions and final state effects. We estimate that the HOMO−LUMO gap for the *p*-benzoquinonemonoimine compounds should retain a value of ca. 5.7−5.9 eV, being robust and stable with little variation for a wide variation of pendent groups, as both the HOMO and LUMO are dominated by molecular orbitals localized on the *p*-benzoquinonemonoimine zwitterion core. For zwitterions **3** and **4**, the observed HOMO−LUMO gaps from the combined photoemission and inverse photoemission slightly differ from the calculated ones. For **3**, we expect a HOMO−LUMO gap of 5.7 eV and observe gap of 5 eV or less, whereas **4** exhibits a larger gap of 6.3 eV, even larger than the calculated value of 5.9 eV. The results are summarized in Table 2.

For the benzyl-substituted zwitterion **5**, the HOMO−LUMO gap is significantly smaller than expected or observed for the other zwitterions. The agreement between the single molecular calculation and the combined photoemission and inverse photoemission spectra HOMO−LUMO gap is quite poor for **5**, unlike the other zwitterions studied (Figure 8). The angle-resolved photoemission spectrum taken at 40 eV (using synchrotron radiation, as opposed to He I radiation used for the other molecules) has been added for **5** (red curve in Figure 8) to confirm that the single molecule calculations fail to provide a good approximation of the HOMO−LUMO gap (red) for this zwitterion. We also found a rigid alignment of the lowest unoccupied molecular orbital just above the substrate Fermi level, that is independent of the zwitterion molecular coverage over a wide range of molecular film thickness (Figure 7b). This is very unusual for molecular adsorbates where final state effects and surface charging have a strong tendency to make the HOMO−LUMO gap appear to increase with increasing film thickness.[36] We found no evidence of surface charging, even at lower temperatures (150 K) and for thick molecular films of **5**, where the film surface is not readily screened by the conducting Au substrate. There is no evidence of a molecular band offset that leads to displacement of the LUMO away from the substrate Fermi level (Figure 7, bottom). This speaks for the possibility of band structure effects, indicative of strong hybridization between molecules that result in extramolecular screening in the photoemission and inverse photoemission final state. The agreement between experimental data and the DFT calculations that include intermolecular band structure effects (BT in Figure 7, bottom) is noticeably satisfactory. Measurements along the k-direction normal to the films of the dispersion of molecular orbital binding energies with the electron wave vector confirm that for this zwitterion **5**, intermolecular band theory applies.[37]

dx.doi.org/10.1021/ja212104b | *J. Am. Chem. Soc.* 2012, 134, 8494−8506

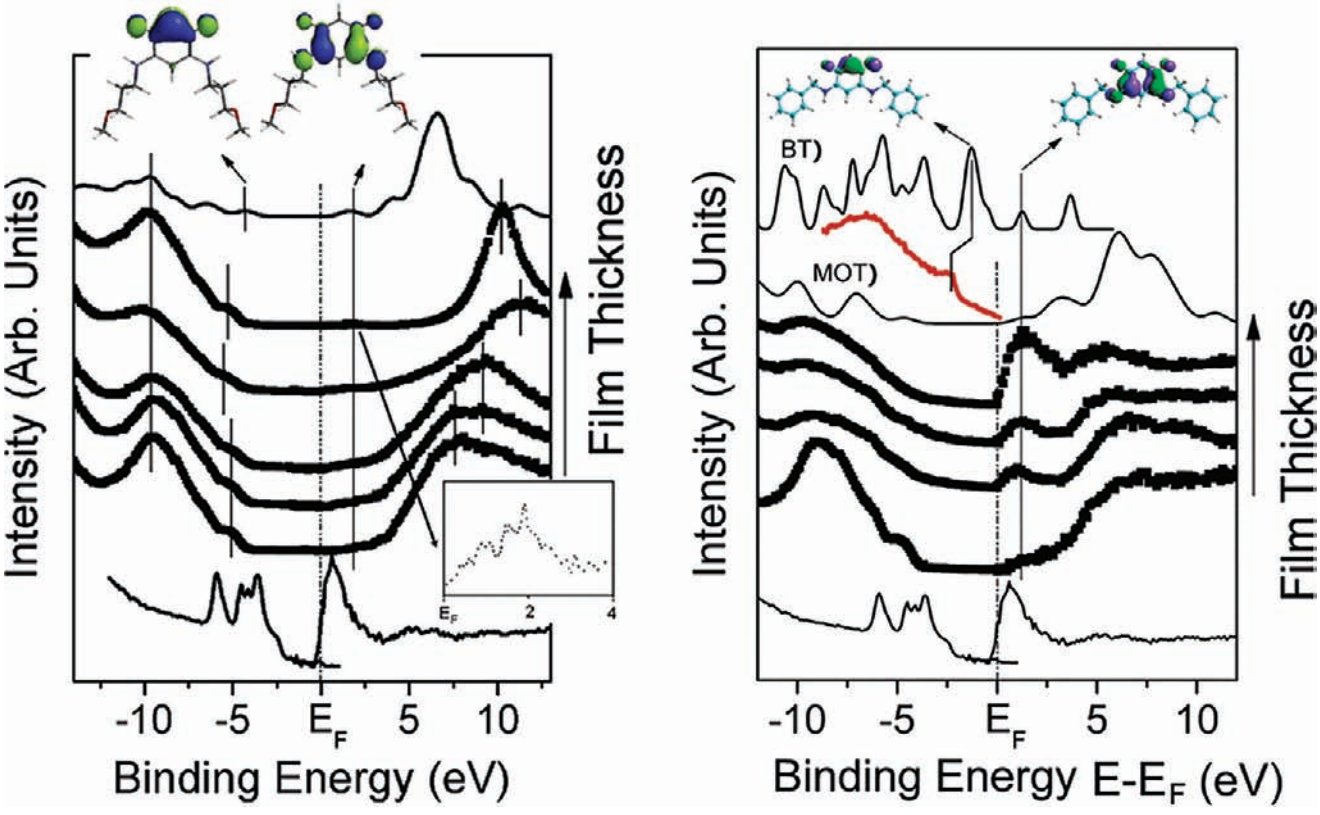

Figure 7. In both figures, the vertical axis indicates increasing film thickness. (Left panel) Combined coverage-dependent photoemission and inverse photoemission spectra (thick lines) of **4** adsorbed on Au at room temperature from solution. The bottom thin line corresponds to the clean Au substrate, taken as reference spectrum. The top thin line is the model calculation of the single molecule density of states, using a semiempirical PM3 approach, uncorrected for matrix elements and final state effects. The vertical lines indicate the position of key spectroscopic features attributable to the adsorbed zwitterion molecular orbitals. Schematics of the HOMO and LUMO orbitals are indicated and identified in the spectra. The HOMO and LUMO levels are depicted by molecular orbital schematics as insets on the top of the figure. The top experimental spectrum is taken from the zwitterion deposited on Au from an ethanol solution instead of the CH_2Cl_2 used for all the other deposited zwitterion films. Some, but not major, changes in the resulting thin films are evident as a function of solvent. The bottom inset is a zoomed region of the unoccupied states, illustrating the position of the LUMO level. (Right panel) The combined coverage-dependent photoemission and inverse photoemission spectra (thick lines) of molecules **5** adsorbed on Au at room temperature. The bottom thin line corresponds to the clean Au substrate, taken as reference spectrum. The top thin lines are the model calculations of the single molecule density of states (MOT), using a semiempirical PM3 approach uncorrected for matrix elements and final state effects and a comparison model calculation of the band structure density of states (BT), using DFT with the known crystal structure data of molecule **5**. The HOMO and LUMO are indicated by vertical bars and depicted by molecular orbital schematics as insets on the top of the figure. Because of the low density of states at the highest occupied molecular orbital (HOMO) for this zwitterion, we used a photon energy of 40 eV (as opposed to He I at 21.2 eV used for the other photoemission spectra), as shown in the red spectrum, to reveal unambiguously the HOMO level energy.

The key experimental finding of photoemission and inverse photoemission data (Figures 7 and 8) is the observation that the position of the Fermi level energy of the Au substrate (used as zero energy reference for the photoemission and inverse photoemission) is very close to the conduction band edge. This is to say that the placement of the lowest unoccupied molecular orbitals (LUMO) of the adsorbed molecules **1**, **2**, **3**, and **5** is very close to the substrate Fermi level. This is consistent with the absence of charging in the thicker molecular films. This noteworthy property is seldom observed in undoped molecular films. In the case of zwitterion **4**, the molecular orbital alignment places the substrate Fermi level within the HOMO−LUMO gap, well separated from the molecular orbital band edges, as is expected for organic dielectric thin films without electronic interaction with the substrate.

We systematically observe very limited charging effects in either photoemission or inverse photoemission for the adsorbed molecules **1**, **2**, **3**, and **5**. The expected final state effects[38] that should occur with increasing molecule films thickness are remarkably small. We infer, therefore, that these molecular films have good charge transfer properties, confirmed by the band alignment between the LUMO of the molecules and the valence band edge of the metallic substrate (Figure 8). We also interpret these results as an indication of the Au substrate acting as an electron donor. This is intuitively reasonable if we consider that in the molecular layers, the positively charged side of the molecular core is situated at a short distance from the interface. From a device point-of-view, we conclude that Au is a well-matched electron injector in these films.

Remarkable electronic properties are specifically found for films of molecule **5** (zwitterion with benzyl R groups), which forms a molecular film that exhibits a density of states overlapping the Fermi level of the Au substrate. The total absence of charging effects, even when cooling down the sample to 100 K, is inconsistent with doped semiconductor properties. The absence of final state effects in either photoemission or inverse photoemission (i.e., with either

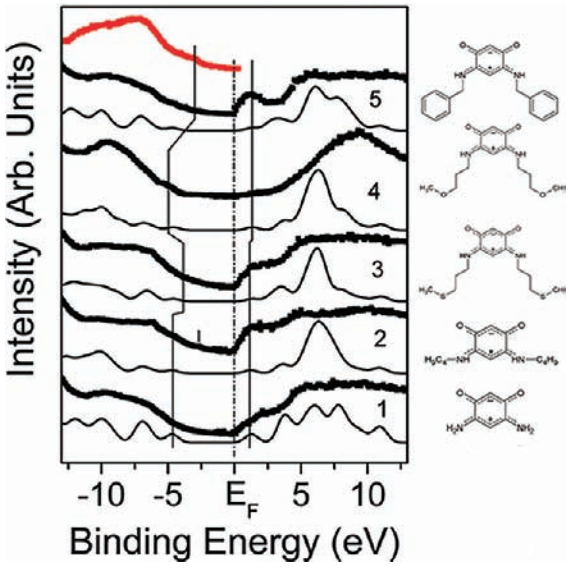

Figure 8. The combined photoemission and inverse photoemission spectra (thick lines) of *p*-benzoquinonemonoimine zwitterions $(C_6H_2(\cdots NHR)_2(\underline{\cdots}O)_2)$, where R = H (**1**), *n*-C_4H_9 (**2**), $C_3H_6-S-CH_3$ (**3**), $C_3H_6-O-CH_3$ (**4**), or $CH_2-C_6H_5$ (**5**) on Au. The film thickness is in the range 1−3 nm. Model calculations of the single molecule density of states, using a semiempirical PM3 approach uncorrected for matrix elements and final state effects, are shown for comparison as a thin line for each species. The right side of the figure shows the schematic structure of each molecule. For the benzyl-substituted zwitterion **5**, the angle-resolved photoemission taken at 40 eV (as opposed to helium I radiation for the other molecules) is also shown.

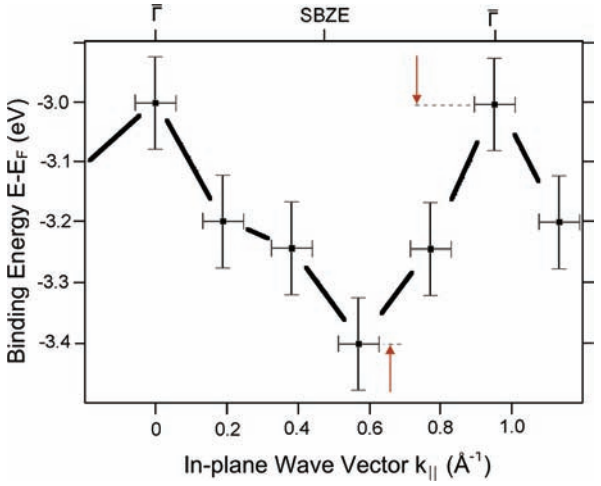

Figure 9. Dispersion of the intermolecular band from the HOMO molecular orbitals of zwitterion **2** molecules assembled on Au(111) in the reduced Brillouin zone scheme. The arrows indicate the extent of the dispersion (or effective bandwidth) of the HOMO along the zwitterion **2** molecular core π stacking direction.

holes or electrons), combined with almost a complete absence of photovoltaic charging, indicates that these molecular films are not dielectrics. This molecule is expected to form n-type semiconductor materials of significant mobility, very close to a semimetal, which is a highly desirable property in the field of molecular electronics.[39] One should recall that the intrinsic molecular dipoles in ultrathin films are expected to differ from the individual molecules properties. This is expected when charge exchange with the substrate occurs (as shown, for example, by XPS data on molecule **2**), or when thin films electronic properties do not match those of individual molecules (as in molecule **5**).

For **5**, the occurrence of available states at the Fermi level of Au is likely related to the crystalline nature of its molecular films. This assumption is confirmed by modeling of the density of states beyond single molecule approximation to account for the observed density of states.[37] This is the only zwitterion within the series investigated where the experimental HOMO−LUMO gap from the combined photoemission and inverse photoemission data is far smaller than suggested by single molecule calculations. DFT calculations, including band structure effects, provide a HOMO−LUMO gap in better agreement with experiment, although it remains too small. This is typical for such DFT calculations.[40]

Self-organization in the packing of ultrathin films, resulting in a crystalline structure, was indeed observed with the butyl and benzyl pendant groups in **2** and **5**, respectively. Figure 9 shows results from band mapping experiments indicating long-range ordering in a direction normal to the zwitterion cores. The emission angle-dependence of photoemission has been exploited to determine the dispersion (change in binding energy) as a function of the wave vector $k_{//}$, parallel to the surface of the film, using the equation:

$$k_{\|} = \sqrt{\frac{2m}{h^2}E_{\mathrm{kin}}}\,\sin(\theta) = 0.512\sqrt{E_{\mathrm{kin}}/\mathrm{eV}}\,\sin(\theta)\text{Å}^{-1}$$

in which the value of $k_{//}$ can be estimated from the photoelectron kinetic energy (E_{kin}) and the photoemission emission angle (θ).[41]

The periodic band dispersion of Figure 9 provides clear evidence of large scale ordered packing of molecule **2**. A dense in-plane packing of adjacent molecules of zwitterion **2** can be inferred from the intermolecular dispersion or bandwidth of about 400 meV, obtained by emission angle-dependent photoemission, as indicated in Figure 9 (arrows). This is a rather large bandwidth (dispersion) for a molecular film, with a related lattice period of 6.4 ± 0.2 Å [$2\pi/k$ (k = 0.98 Å^{-1})], in a direction parallel to the Au surface. This lattice spacing relates to an intermolecular spacing of ca. 3.2 ± 0.2 Å, with two molecules per period. This is consistent with the picture of molecules of **2** having their cores standing approximately normal to the surface, as discussed previously,[20] and packed

Table 2. Molecular Band Offsets and HOMO LUMO Gaps (in eV)

Molecule	1	2	3	4	5
LUMO expt.	1.4 ± 0.3	1.4 ± 0.2	1.5 ± 0.2	1.4 ± 0.3	1.1 ± 0.2
HOMO expt.	4.5 ± 0.3	4.5 ± 0.1	3.2 ± 0.1	4.9 ± 0.1	2.5 ± 0.3
HOMO−LUMO gap (expt.)	5.9 ± 0.5	5.9 ± 0.1	<5	6.3 ± 0.3	3.6 ± 0.3
Theory PM3, gap value	5.8	5.8	5.7	5.9	5.9
Theory−DFT for the solid-gap value		-	-	-	1.63

dx.doi.org/10.1021/ja212104b | J. Am. Chem. Soc. 2012, 134, 8494−8506

with spacings values corresponding to those found in the crystalline state (Figure 3). This short distance opens the possibility of $\pi-\pi$ stacking allowing good mobility charge transport.

Direct measurement of the electrical transport properties of these ultrathin films is challenging, especially when considering that these zwitterion molecules do not all adsorb on insulating substrates. We have no experimental indication that molecular films of quality approaching those on Au can be realized on insulating substrates, and the AFM imaging on mica showed possible nonuniform coverage. For example, we identified by IR microscopy that **4** did not adsorb on SiO_2, whereas it preferentially covers the nearby Au patterns (Figure 10).

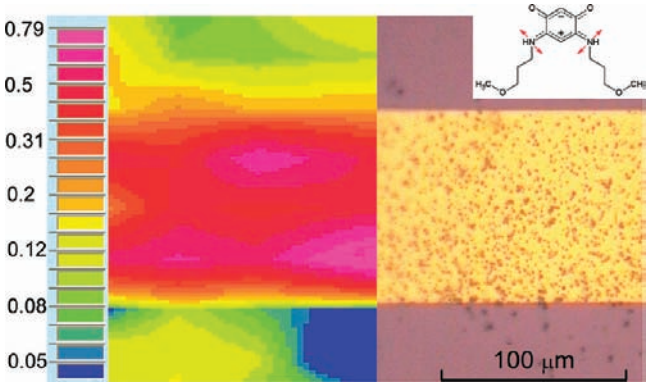

Figure 10. Preferred adsorption of molecule **4** on a Au stripe over a native silicon oxide surface. On the right-hand side, the image of the Au stripe is shown, and on the left side, that of the IR map based on the vibrational mode absorption at 3130 cm^{-1}. This energy is characteristic of the symmetric wagging mode of the *p*-benzoquinonemonoimine zwitterions, as indicated in the inset. The color scale indicates the absorption strength. The inhomogeneous appearance of the surface relates to a lightly ethanol washed substrate, in order to get a reasonable signal-to-noise ratio in the pixelized IR data acquisition.

While no XPS data indicate strong chemisorption of **4** on Au, the IR mapping of Figure 10 validates the affinity of this molecule for Au. Compound **2** adsorbs on both Au and SiO_2 substrates, although adsorption on the latter is sensitive to details on the oxide surface. We therefore tested this molecule for transport measurements.

We fabricated electrodes nanogaps structures, with a distance not exceeding a few nanometers between two Au contacts on a microfluidic-equipped chip allowing chemical exposure and cleaning of the nanogaps.[42] Figure 11 shows that significant current flow can be established in junctions made of a few molecules, especially when compared to dodecanedithiol, used as benchmark of molecular transport.[43] Measurements were performed on samples that were immersed overnight in solutions containing the zwitterions, and washed in a microfluidic channel. We found that the solvent flow speed should not exceed 0.01 m/s, in order to maintain electrical interconnects. We conclude that the electrical transport through molecules **2** is robust and significantly larger than what is observed in alkane thiols. While it may not be surprising that such molecules are better conductors than alkanes. This test experiment is encouraging and adds confidence in the claims of good charge transport properties through an ensemble of zwitterion molecules of the type studied.[44]

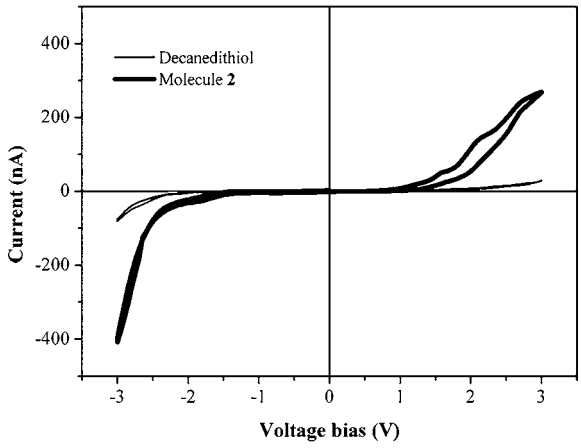

Figure 11. Current/voltage curve of molecule **2**, compared with decanedithiol molecules trapped between Au electrodes separated by 1−3 nm. A gain of nearly 1 order of magnitude is found (with the hysteresis in the I/V curve being likely related to charge trapping by the SiO_2 substrate or solvent traces).

CONCLUSION

We have shown that small molecules of the *p*-benzoquinonemonoimine type, with significant intrinsic dipoles over short distance, can be adsorbed on conducting surfaces. By combining the experimental results from several different surface characterization techniques, we have provided compelling evidence that very thin films (less than 2 nm), with high surface coverage (only few pinholes) can be successfully obtained. The results are very reproducible as they do not depend critically on the details of a surface functionalization process, kept simple. Good interface screening properties are illustrated by thickness-dependent studies, showing limited change of the electronic spectroscopic features, with a good agreement between experimental spectra and simplest models of single molecule energies. Benzyl, butyl and methoxy substituents are not considered, a priori, as strong anchoring groups (although aromatic substituents may develop interactions with Au),[45] but their presence on the zwitterion N-substituent provides some important features. First, these groups interact with the Au surface and help to stabilize the molecule on the surface. In previous work, we observed some participation of the alkyl substituents in a surprisingly strong anchoring of butyl-substituted zwitterions on Au.[20] Second, the N-substituent influences the molecular organization on the surface. For example, the steric hindrance of the group may lead to increased distances between adjacent molecules, or well-organized structures can result from π-stacking.[46] We find that crystalline ordering of the *p*-benzoquinonemonoimine molecules is possible, with the related π-stacking promoting conductivity in the thin films that was mostly evidenced by the occurrence of molecular density of states at the substrate Fermi level. These interface molecular films can therefore play an important role for organic electronics devices, creating ideally a highly conductive interface with metallic electrodes, promoting efficient carrier injection into an organic film. Future work could also take advantage of the coordination properties of these zwitterions toward transition metals to create metal-containing thin layers on surfaces.

dx.doi.org/10.1021/ja212104b | *J. Am. Chem. Soc.* 2012, 134, 8494−8506

■ ASSOCIATED CONTENT

Supporting Information

^{1}H and $^{13}C\{^{1}H\}$ NMR and mass spectrometry data for zwitterions **3** and **4**, crystallographic details for **2**, **3**, and **4**, comparison of the XPS signals, ORTEP and packing of **2** and **4**, AFM of Au surface and attempts to synthesize **6** and **7**. This material is available free of charge via the Internet at http://pubs.acs.org.

■ AUTHOR INFORMATION

Corresponding Author

braunstein@unistra.fr; pdowben@unl.edu; bdoudin@unistra.fr

Notes

The authors declare no competing financial interest.

■ ACKNOWLEDGMENTS

This research was supported by the National Science Foundation through grants number CHE-0909580 and DMR-0851703, the Centre National de la Recherche Scientifique and the Ministère de la Recherche et des Nouvelles Technologies (Paris), the ANR (07-BLAN-0274-04), and the Nebraska Center for Materials and Nanoscience at University of Nebraska—Lincoln. The authors acknowledge the assistance of Yaroslav Losovyj and Orhan Kizilkaya with the angle-resolved photoemission and spatial infrared spectromicroscopy studies, respectively. Some measurements were performed at the Center for Advanced Microstructure and Devices, which is supported by the Louisiana Board of Regents. The support of the STnano cleanroom facilities (H. Majjad, S. Siegwald) is also gratefully acknowledged.

■ REFERENCES

(1) Braun, S.; Salaneck, W. R.; Fahlman, M. *Adv. Mater.* **2009**, *21*, 1450−1472.

(2) Karthäuser, S. *J. Phys.: Condens. Matter* **2011**, *23*, 013001.

(3) Ma, H.; Yip, H.-L.; Huang, F.; Jen, A. K.-Y. *Adv. Funct. Mater.* **2010**, *20*, 1371−1388.

(4) Hill, I. G.; Rajagopal, A.; Kahn, A.; Hu, Y. *Appl. Phys. Lett.* **1998**, *73*, 662−664.

(5) Ishii, H.; Sugiyama, K.; Ito, E.; Seki, K. *Adv. Mater.* **1999**, *11*, 605−625.

(6) Zhu, X. Y. *Surf. Sci. Rep.* **2004**, *56*, 1−83.

(7) Koch, N.; Elschner, N.; Schwartz, J.; Kahn, A. *Appl. Phys. Lett.* **2003**, *82*, 2281−2883.

(8) Kera, S.; Yabuuchi, Y.; Yamane, H.; Setoyama, H.; Okudaira, K. K.; Kahn, A.; Ueno, N. *Phys. Rev. B* **2004**, *70*, 085304/1−085304/6.

(9) Dowben, P. A.; Rosa, L. G.; Ilie, C. C.; Xiao, J. *J. Electron Spectrosc. Relat. Phenom.* **2009**, *174*, 10−21.

(10) L'vov, V. S.; Naaman, R.; Tiberkevich, V.; Vager, Z. *Chem. Phys. Lett.* **2003**, *381*, 650−653.

(11) Cahen, D.; Naaman, R.; Vager, Z. *Adv. Funct. Mater.* **2005**, *15*, 1571−1578.

(12) Balaz, S.; Caruso, A. N.; Platt, N. P.; Dimov, D. I.; Boag, N. M.; Brand, J. I.; Losovyj, Y. B.; Dowben, P. A. *J. Phys. Chem. B* **2007**, *111*, 7009−7016.

(13) Barraud, C.; Seneor, P.; Mattana, R.; Fusil, S.; Bouzehouane, K.; Deranlot, C.; Graziosi, P.; Hueso, L.; Bergenti, I.; Dediu, V.; Petroff, P; Fert, A. *Nat. Phys.* **2010**, *6*, 615−620.

(14) Yuan, Y.; Reece, T. J.; Sharma, P.; Poddar, S.; Ducharme, S.; Gruverman, A.; Yang, Y.; Huang, J. *Nat. Mater.* **2011**, *10*, 296−302.

(15) (a) Sawicka, A.; Skurski, P.; Simons, J. *Chem. Phys. Lett.* **2002**, *362*, 527−533. (b) Haas, Y.; Zilberg, S. *J. Am. Chem. Soc.* **2004**, *126*, 8991−8998.

(16) Siri, O.; Braunstein, P. *Chem. Commun.* **2002**, 208−209.

(17) (a) Braunstein, P.; Siri, O.; Taquet, J.-P.; Rohmer, M.-M.; Bénard, M.; Welter, R. *J. Am. Chem. Soc.* **2003**, *125*, 12246−12256. (b) Braunstein, P.; Siri, O.; Steffanut, P.; Winter, M.; Yang, Q.-Z. *C. R. Chim.* **2006**, *9*, 1493−1499. (c) Braunstein, P.; Siri, O.; Taquet, J.-p.; Yang, Q.-Z. *Angew. Chem., Int. Ed.* **2006**, *45*, 1393−1397. (d) Taquet, J.-p.; Siri, O.; Braunstein, P.; Welter, R. *Inorg. Chem.* **2004**, *43*, 6944−6953. (e) Yang, Q.-Z.; Kermagoret, A.; Agostinho, M.; Siri, O.; Braunstein, P. *Organometallics* **2006**, *25*, 5518−5527.

(18) (a) Yang, Q.-Z.; Siri, O.; Braunstein, P. *Chem. Commun.* **2005**, 2660−2662. (b) Yang, Q.-Z.; Siri, O.; Brisset, H.; Braunstein, P. *Tetrahedron Lett.* **2006**, *47*, 5727−5731.

(19) Yang, Q.-Z.; Siri, O.; Braunstein, P. *Chem.—Eur. J.* **2005**, *11*, 7237−7246.

(20) Xiao, J.; Zhang, Z.; Wu, D.; Routaboul, L.; Braunstein, P.; Doudin, B.; Losovyj, Y. B.; Kizilkaya, O.; Rosa, L. G.; Borca, C. N.; Gruverman, A.; Dowben, P. A. *Phys. Chem. Chem. Phys.* **2010**, *12*, 10329−10340.

(21) (a) Lu, X.; Hipps, K. W.; Wang, X. D.; Mazur, U. *J. Am. Chem. Soc.* **1996**, *118*, 7197−7202. (b) Xiao, J.; Dowben, P. A. *J. Mater. Chem.* **2009**, *19*, 2172−2178. (c) Dowben, P. A.; Xiao, J.; Xu, B.; Sokolov, A.; Doudin, B. *Appl. Surf. Sci.* **2008**, *254*, 4238−424.

(22) (a) Fang, Y.; Nguyen, P.; Ivasenko, O.; Aviles, M. P.; Kebede, E.; Askari, M. S.; Ottenwaelder, X.; Ziener, U.; Siri, O.; Cuccia, L. A. *Chem Commun.* **2011**, *47*, 11255−11257. (b) Zhang, Z.; Alvira, J.; Barbosa, X.; Rosa, L. G.; Routaboul, L.; Braunstein, P.; Doudin, B.; Dowben, P. A. *J. Phys. Chem. C* **2011**, *115*, 2812−2818.

(23) *Kappa CCD Operation Manual*; Nonius BV: Delft, The Netherlands, 1997; Sheldrick, G. M. *SHELXL97*, Program for the Refinement of Crystal Structures; University of Gottingen, Germany, 1997.

(24) (a) Dowben, P. A; Miller, A., Eds.; *Surface Segregation Phenomena*; CRC Press: Boston, MA,1990; p 145; (b) Cumpson, P. J. *J. Electron Spectrosc. Relat. Phenom.* **1995**, *73*, 25−52. (c) Jablonski, A.; Powell, C. J. *Surf. Sci. Rep.* **2002**, *47*, 33. (d) Tanuma, S.; Powell, C. J.; Penn, D. R. *Scanning* **2006**, *28*, 112−113. (e) Hajati, S.; Coultas, S.; Blornfield, C.; Tougaard, S. *Surf. Interface Anal.* **2008**, *40*, 688−691. (f) Hajati, S.; Tougaard, S. *Anal. Bioanal. Chem.* **2010**, *396*, 2741−2755. (g) Tougaard, S.; Jablonski, A. *J. Vac. Sci. Technol., A* **2011**, *29*, 051401.

(25) (a) Kizilkaya, O.; Scott, J. D.; Morikawa, E.; Garber, J. D.; Perkins, R. S. *Rev. Sci. Instrum.* **2005**, *76*, 13703. (b) Kizilkaya, O.; Prange, A.; Steiner, U.; Oerke, E. C.; Scott, J. D.; Morikawa, E.; Hormes, J. *Nucl. Instrum. Methods Phys. Res., Sect. A* **2007**, *582*, 274−276.

(26) Delley, B. *J. Chem. Phys.* **1990**, *92*, 508. Delley, B. *J. Chem. Phys.* **2000**, *113*, 7756.

(27) (a) Vericat, C.; Vela, M. E.; Benitez, G. A.; Gago, J. A. M.; Torrelles, X.; Salvarezza, R. C. *J. Phys.: Condens. Matter* **2006**, *18*, R867−R900. (b) Vericat, C; Vela, M. E.; Andreasen, G.; Salvarezza, R. C.; Vazquez, L.; Marin-Gago, J. A. *Langmuir* **2001**, *17*, 4919−4924.

(28) (a) Kriegisch, V.; Lambert, C. *Top. Curr. Chem.* **2005**, *258*, 257−313. (b) Tao, F.; Bernasek, S. L. *Chem. Rev.* **2007**, *107*, 1408−1453. (c) Love, J. C.; Estroff, L. A.; Kriebel, J. K.; Nuzzo, R. G.; Whitesides, G. M. *Chem. Rev.* **2005**, *105*, 1103−1169. (d) Nuzzo, R. G.; Allara, D. L. *J. Am. Chem. Soc.* **1983**, *105*, 4481−4483. (e) Nuzzo, R. G.; Zegarski, B. R.; Dubois, L. H. *J. Am. Chem. Soc.* **1987**, *109*, 733−40. (f) Vericat, C.; Vela, M. E.; Benitez, G.; Carro, P.; Salvarezza, R. C. *Chem. Soc. Rev.* **2010**, *39*, 1805−1834.

(29) (a) Weidner, T.; Kraemer, A.; Bruhn, C.; Zharnikov, M.; Shaporenko, A.; Siemeling, U.; Traeger, F. *Dalton Trans.* **2006**, 2767−2777. (b) Mannini, M.; Sorace, L.; Gorini, L.; Piras, F. M.; Caneschi, A.; Magnani, A.; Menichetti, S.; Gatteschi, D. *Langmuir* **2007**, *23*, 2389−2397. (c) Noh, J.; Jeong, Y.; Ito, E.; Hara, M. *J. Phys. Chem. C* **2007**, *111*, 2691−2695. (d) Jian, H.; Tour, J. M. *J. Org. Chem.* **2003**, *68*, 5091−5103. (e) Cavalleri, O.; Vignolo, M.; Strano, G.; Natale, C.; Rolandi, R.; Thea, S.; Prato, M.; Gonella, G.; Canepa, M.; Gliozzi, A. *Bioelectrochemistry* **2004**, *63*, 3−7. (f) Tierney, H. L.; Baber, A. E.; Sykes, E. C. H.; Akimov, A.; Kolomeisky, A. B. *J. Phys. Chem. C* **2009**, *113*, 10913−10920. (g) Baber, A. E.; Tierney, H. L.; Sykes, E. C. H.

ACS Nano **2008**, *2*, 2385−2391. (h) Menozzi, E.; Pinalli, R.; Speets, E. A.; Ravoo, B. J.; Dalcanale, E.; Reinhoudt, D. N. *Chem.—Eur. J.* **2004**, *10*, 2199−2206. (i) Zhang, S.; Echegoyen, L. *Tetrahedron* **2006**, *62*, 1947−1954. (j) Mannini, M.; Rovai, D.; Sorace, L.; Perl, A.; Ravoo, B. J.; Reinhoudt, D. N.; Caneschi, A. *Inorg. Chim. Acta* **2008**, *361*, 3525−3528.

(30) Jewell, A. D.; Tierney, H. L.; Baber, A. E.; Iski, E. V.; Laha, M. M.; Sykes, E. C. H. *J. Phys.: Condens. Matter* **2010**, *22*, 264006/1−264006/11.

(31) Bellisario, D. O.; Jewell, A. D.; Tierney, H. L.; Baber, A. E.; Sykes, E. C. H. *J. Phys. Chem. C* **2010**, *114*, 14583−14589.

(32) (a) Tierney, H. L.; Jewell, A. D.; Baber, A. E.; Iski, E. V.; Sykes, E. C. H. *Langmuir* **2010**, *26*, 15350−15355. (b) Zharnikov, M; Golzhauser, A.; Grunze, M. *Appl. Phys. Lett.* **1999**, *75*, 2401−2403.

(33) Dezarnaud, C.; Tronc, M.; Modelli, A. *Chem. Phys.* **1991**, *156*, 129−140.

(34) (a) Zoloff Michoff, M. E.; Velez, P.; Leiva, E. P. M *J. Phys. Chem. C* **2009**, *113*, 3850−3854. (b) Iori, F.; Corni, S.; Di Felice, R. *J. Phys. Chem. C* **2008**, *112*, 13540−13545. (c) Cafe, P. F.; Larsen, A. G.; Yang, W.; Bilic, A.; Blake, I. M.; Crossley, M. J.; Zhang, J.; Wackerbarth, H.; Ulstrup, J.; Reimers, J. R. *J. Phys. Chem. C* **2007**, *111*, 17285−17296. (d) Gong, J.; Yan, T.; Mullins, C. B. *Chem. Commun.* **2009**, 761−763. (e) Sivanesan, A.; John, S. A. *Langmuir* **2008**, *24*, 2186−2190. (f) Barber, M.; Conner, J. A.; Guest, M. F.; Hillier, I. H.; Schwarz, M.; Stacy, M. *J. Chem. Soc., Faraday Trans. 2* **1973**, *69*, 551−558. (g) Lindberg, B. J.; Hedman, J. *Chem. Scr.* **1975**, *7*, 155−166. (h) Yoshida, T.; Sawada, S. *Bull. Chem. Soc. Jpn.* **1974**, *47*, 50−53. (i) Yatsimirskii, K. B.; Nemoshalenko, V. V.; Aleshin, V. G.; Bratushko, Y. I.; Moiseenko, E. P. *Chem. Phys. Lett.* **1977**, *52*, 481−484.

(35) (a) Lindberg, B. J.; Hamrin, K.; Johansson, G.; Gelius, V.; Falhlmann, A.; Nordling, C.; Siegbahn, K. *Phys. Scr.* **1970**, *1*, 286−298. (b) Block, E. *Reactions of Organosulfur Compounds*; Academic Press: New York, 1978.

(36) (a) Sato, N.; Seki, K.; Inokuchi, H. J. *J. Chem. Soc., Faraday Trans. 2* **1981**, *77*, 1621−1633. (b) Fukagawa, H.; Yamane, H.; Kataoka, T.; Kera, S.; Nakamura, M.; Kudo, K.; Ueno, N. *Phys. Rev. B* **2006**, *73*, 245310/1−245310/5. (c) Schroeder, P. G.; France, C. B.; Park, J. B.; Parkinson, B. A. *J. Phys. Chem. B* **2003**, *107*, 2253−2261.

(37) Rosa, L. G.; Velev, J.; Zhang, Z.; Alvira, J.; Vega, O.; Diaz, G.; Routaboul, L.; Braunstein, P.; Doudin, B.; Losovyj, Ya. B.; Dowben, P. A. *Phys. Status Solidi B* **2012**, DOI: 10.1002/pssb.201147426.

(38) (a) Ortega, J. E.; Himpsel, F. J.; Li, D.; Dowben, P. A. *Solid State Commun.* **1994**, *91*, 807. (b) Dowben, P. A. *Surf. Sci. Rep.* **2000**, *40*, 151−247.

(39) Chua, L.-L.; Zaumseil, J.; Chang, J.-F.; Ou, E. C.-W.; Ho, P. K.-H.; Sirringhaus, H.; Friend, R. H. *Nature* **2005**, *434*, 194−199.

(40) (a) Kümmel, S.; Kronik, L. *Rev. Mod. Phys.* **2008**, *80*, 3−60. (b) Bechstedt, F.; Fuchs, F.; Kresse, G. *Phys. State Solidi B* **2009**, *246*, 1877−1892. (c) Stein, T.; Kronik, L.; Baer, R. *J. Am. Chem. Soc.* **2009**, *131*, 2818. (d) Liao, M.-S.; Lu, Y.; Scheiner, S. *J. Comput. Chem.* **2003**, *24*, 623−631. (e) Yakovkin, I. N.; Dowben, P. A. *Surf. Rev. Lett.* **2007**, *14*, 481−487.

(41) (a) Dowben, P. A.; Xu, B.; Choi, J.; Morikawa, E. *Handb. Thin Film Mater.* **2002**, *2*, 61−113. (b) Plummer, E. W.; Eberhardt, W. *Adv. Chem. Phys.* **1982**, *49*, 533−656. (c) Steinrück, H.-P. *Vacuum* **1994**, *45*, 715−731.

(42) Lunca Popa, P.; Dalmas, G.; Faramarzi, V.; Dayen, J. F.; Majjad, H.; Kemp, N. T.; Doudin, B. *Nanotechnology* **2011**, *22*, 215302.

(43) Akkerman, H. B.; de Boer, B. *J. Phys.: Condens. Matter* **2008**, *20*, 013001.

(44) Doudin, B.; Braunstein, P.; Routaboul, L.; Dalmas, G.; Zhang, Z.; Dowben, P. Patent WO 2012025878 A1 to CNRS.

(45) (a) Britton, A. J.; Rienzo, A.; O'Shea, J. N.; Schulte, K. *J. Chem. Phys.* **2010**, *133*, 094705/1−094705/7. (b) Chen, W.-K.; Cao, M.-J.; Liu, S.-H.; Lu, C.-H.; Xu, Y.; Li, J.-Q. *Chem. Phys. Lett.* **2006**, *417*, 414−418. (c) Gao, P.; Weaver, M. J. *J. Phys. Chem.* **1985**, *89*, 5040−5046. (d) Schuster, C.; Schwingenschloegl, U. *Chem. Phys. Lett.* **2009**, *468*, 75−78. (e) Syomin, D.; Kim, J.; Koel, B. E.; Ellison, G. B. *J. Phys. Chem. B* **2001**, *105*, 8387−8394.

(46) (a) Brede, J.; Linares, M.; Kuck, S.; Schwoebel, J.; Scarfato, A.; Chang, S.-H.; Hoffmann, G.; Wiesendanger, R.; Lensen, R.; Kouwer, P. H. J.; Hoogboom, J.; Rowan, A. E.; Bröring, M.; Funk, M.; Stafström, S.; Zerbetto, F.; Lazzaroni, R. *Nanotechnology* **2009**, *20*, 275602/1−275602/10. (b) Guaino, P.; Carty, D.; Hughes, G.; McDonald, O.; Cafolla, A. A. *Appl. Phys. Lett.* **2004**, *85*, 2777−2779. (c) Han, B.; Li, Z.; Wandlowski, T.; Blaszczyk, A.; Mayor, M. *J. Phys. Chem. C* **2007**, *111*, 13855−13863. (d) Huang, T.; Hu, Z.; Zhao, A.; Wang, H.; Wang, B.; Yang, J.; Hou, J. G. *J. Am. Chem. Soc.* **2007**, *129*, 3857−3862. (e) Jiang, P.; Deng, K.; Fichou, D.; Xie, S.-S.; Nion, A.; Wang, C. *Langmuir* **2009**, *25*, 5012−5017. (f) Langlais, V. A.; Gauthier, Y.; Belkhir, H.; Maresca, O. *Phys. Rev. B* **2005**, *72*, 085444/1−085444/7. (g) Lux, F.; Lemercier, G.; Andraud, C.; Schull, G.; Charra, F. *Langmuir* **2006**, *22*, 10874−10876. (h) Pinheiro, L. S.; Temperini, M. L. A. *Surf. Sci.* **2000**, *464*, 176−182. (i) Sakai, N.; Sisson, A. L.; Buergi, T.; Matile, S. *J. Am. Chem. Soc.* **2007**, *129*, 15758−15759. (j) Sisson, A. L.; Sakai, N.; Banerji, N.; Fuerstenberg, A.; Vauthey, E.; Matile, S. *Angew. Chem., Int. Ed.* **2008**, *47*, 3727−3729. (k) Tulevski, G. S.; Bushey, M. L.; Kosky, J. L.; Ruter, S. J. T.; Nuckolls, C. *Angew. Chem., Int. Ed.* **2004**, *43*, 1836−1839.